Two-photon and three-photon spectroscopy of ZnO under uniaxial stress

J. Wrzesinski and D. Fröhlich
Institut für Physik, Universität Dortmund, D-44221 Dortmund, Germany
(Received 25 June 1997)

Using two-photon excitation spectroscopy and three-photon difference frequency generation, resonances on the transverse and longitudinal polariton branches of the $A(\Gamma_5)$, $B(\Gamma_5)$, and $C(\Gamma_1)$ $1S$ excitons of ZnO are studied under uniaxial stress. Due to the small linewidth, shifts and splittings are clearly resolved and six deformation potentials are determined with high accuracy. [S0163-1829(97)06944-0]

I. INTRODUCTION

Semiconductors of large band gap have gained increasing interest because they are used for the construction of blue light-emitting luminescence and even laser diodes. There is a competition between II-VI and III-V semiconductors.[1,2] The II-VI devices are based on ZnSe, which crystallizes in zinc-blende structure, whereas the III-V devices are based on GaN, which crystallizes in wurtzite structure. By epitaxial growth on GaAs it can also be forced into zinc-blende structure.[3] Concerning the fundamental electronic properties like valence-band structure and details of excitonic spectra the zinc-blende semiconductors are much better known than the wurtzite materials. This is especially true for the deformation potentials, which are gained from measurements under hydrostatic[4–6] and uniaxial stress.[7–9] Because of the more complicated valence-band structure one expects in wurtzite materials at least six deformation potentials as compared to three in zinc-blende materials. For the determination of these six deformation potentials one needs rather large crystals in order to apply uniaxial stress in different directions with respect to the crystalline axes. Unfortunately GaN single crystals of sufficient size (several millimeters) have not been available up to now. We have chosen ZnO as a model substance for the determination of deformation potentials in a wurtzite structure by nonlinear spectroscopy because ZnO exhibits optical properties similar to those observed in GaN.[10] We will show that four configurations of applying the force to the crystal and choosing the total $\vec{k}$ vector are sufficient to determine the six deformation potentials. We furthermore show that the influence of seven further deformation potentials can be neglected.

The paper is organized as follows. After a short description of the experimental setup, we present an outline of the theory for the analysis of our data. Finally, experimental results are presented and discussed.

II. EXPERIMENT

Two-photon excitation spectroscopy (2P-ES) and three-photon difference frequency generation (3P-DFG) are performed with a tunable dye laser pumped by a Nd:YAG laser with a repetition rate of 10 Hz. The lasers have a pulse length of 5 ns and a peak energy of 8 mJ (dye laser) and 600 mJ (Nd:YAG laser). For the 3P-DFG measurements of some of the resonances on the lower polariton branches the photon energy of the Nd:YAG laser ($\hbar\omega_1 = 1.164\,75$ eV) is shifted by stimulated Raman effect in methane or hydrogen to $\hbar\omega_2 = 0.803\,43$ eV or $\hbar\omega_3 = 0.649\,72$ eV, respectively. For three-photon difference frequency generation the direction of the infrared laser beam is antiparallel to the dye laser. Both laser beams are focused on the sample, which is mounted in the uniaxial stress apparatus in a helium flow cryostat (Janis model DT) at a temperature of about 5 K. The polarization directions of the laser beams are adjustable by half-wave plates. A double-prism monochromator (Zeiss MM3) is used to suppress scattered light from the dye laser. The electronic signals of the signal photomultiplier and the reference diodes are measured by gated integrators, digitized by analog-to-digital converters, and recorded by a computer, which also controls the wavelength setting and the polarization of the laser.

The samples are single crystals and oriented to better than 0.05° by x-ray Bragg reflection. The surfaces are polished and etched. Typically dimensions of the crystals after preparation are about $1.5\times1.5\times6$ mm^3.

Measurements are performed in four different configurations I, II, III, and IV (Fig. 1) which are specified by the directions of the applied force $\vec{\tau}$ and total $\vec{k}$ vector with respect to the crystalline axes: configuration I, $\vec{\tau}\|[000\underline{1}]$ (z axis) and $\vec{k}\|[11\underline{2}0]$ (x axis); configuration II, $\vec{\tau}\|[10\bar{1}0]$ (y

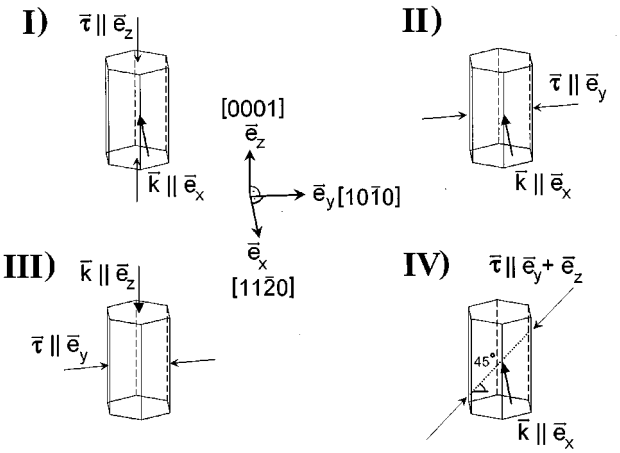

FIG. 1. Schematic diagram of the four experimental configurations I–IV. $\vec{\tau}$ and $\vec{k}$ are the applied force and the total $\vec{k}$ vector, respectively.

axis) and $\vec{k}\|[11\bar{2}0]$; configuration III, $\vec{\tau}\|[10\bar{1}0]$ and $\vec{k}\|[\underline{0}001]$; configuration IV, $\vec{\tau}$ under 45° between $[0001]$ and $[10\underline{1}0]$, $\vec{k}\|[11\underline{2}0]$. The two- and three-photon spectra are measured for uniaxial stress up to 500 MPa. The uncertainty in the stress values is less than 2 MPa.

III. THEORY

The exciton and polariton states are derived from the lowest *s*-like conduction band and the *p*-like valence bands. Without spin-orbit coupling the crystal-field causes a splitting of the *p* states into Γ_5 and Γ_1 states. Crystal-field splitting *and* spin-orbit coupling lead to three twofold degenerate valence bands. These bands are denoted $A(\Gamma_7)$, $B(\Gamma_9)$, and $C(\Gamma_7)$ in order of increasing energy. The symmetry of the excitons with a 1*S* envelope (symmetry Γ_1) can be decomposed into irreducible components (following the notation of Ref. 12)

TABLE I. Components of the strain tensor for different stress directions.

	$\vec{\tau}\|\vec{e}_z$	$\vec{\tau}\|\vec{e}_y$	$\vec{\tau}\|(\vec{e}_y+\vec{e}_z)$
ϵ_{zz}	$S_{33}\tau$	$S_{13}\tau$	$(S_{13}+S_{33})\tau/2$
$\epsilon_{xx}+\epsilon_{yy}$	$2S_{13}\tau$	$(S_{12}+S_{11})\tau$	$[(S_{12}+S_{11})/2+S_{13}]\tau$
$\epsilon_{xx}-\epsilon_{yy}$	0	$(S_{12}-S_{11})\tau$	$(S_{12}-S_{11})\tau/2$
ϵ_{yz}	0	0	$S_{44}\tau/2$
ϵ_{xz}	0	0	0
ϵ_{xy}	0	0	0

$$A \text{ excitons:} \quad \Gamma_1\otimes\Gamma_7\otimes\Gamma_7=\Gamma_5\oplus\Gamma_1\oplus\Gamma_2, \tag{1}$$

$$B \text{ excitons:} \quad \Gamma_1\otimes\Gamma_7\otimes\Gamma_9=\Gamma_5\oplus\Gamma_6, \tag{2}$$

$$C \text{ excitons:} \quad \Gamma_1\otimes\Gamma_7\otimes\Gamma_7=\Gamma_1\oplus\Gamma_5\oplus\Gamma_2. \tag{3}$$

TABLE II. Hamiltonian matrix for 1*S* excitons in wurtzite semiconductors (pointgroup C_{6v}) for $\vec{k}=\vec{0}$. Γ_i denote the symmetry of the wave functions ψ_i.

Γ_i	Γ_5	Γ_5	Γ_5	Γ_5	Γ_5	Γ_5	Γ_1	Γ_1	Γ_2	Γ_6	Γ_6	Γ_2
ψ_i:	X_A	X_B	X_C	Y_A	Y_B	Y_C	Z_A	Z_C	T_A	T_{B_1}	T_{B_2}	T_C
X_A	$A+\Delta_{A5}$	Δ_{1+}	Δ_2	0	Σ_4	0	0	Σ_5	0	Σ_6	Σ_7	Σ_8
X_B	Δ_{1+}	$B+\Delta_{B5}$	Δ_{3+}	Σ_4	0	Σ_9	$-\Sigma_7$	Σ_{10}	$-\Sigma_6$	0	0	Σ_{11}
X_C	Δ_2	Δ_{3+}	$C+\Delta_{C5}$	0	Σ_9	0	Σ_5	0	Σ_8	Σ_{11}	Σ_{10}	0
Y_A	0	Σ_4	0	$A+\Delta_{A5}$	Δ_{1-}	Δ_2	0	Σ_8	0	$-\Sigma_7$	Σ_6	$-\Sigma_5$
Y_B	Σ_4	0	Σ_9	Δ_{1-}	$B+\Delta_{B5}$	Δ_{3-}	Σ_6	$-\Sigma_{11}$	$-\Sigma_7$	0	0	Σ_{10}
Y_C	0	Σ_9	0	Δ_2	Δ_{3-}	$C+\Delta_{C5}$	Σ_8	0	$-\Sigma_5$	$-\Sigma_{10}$	Σ_{11}	0
Z_A	0	$-\Sigma_7$	Σ_5	0	Σ_6	Σ_8	$A+\Delta_{A1}$	Δ_4	0	$-\Sigma_4$	Σ_1	0
Z_C	Σ_5	Σ_{10}	0	Σ_8	$-\Sigma_{11}$	0	Δ_4	$C+\Delta_{C1}$	0	Σ_9	$-\Sigma_3$	0
T_A	0	$-\Sigma_6$	Σ_8	0	$-\Sigma_7$	$-\Sigma_5$	0	0	$A+\Delta_{A2}$	Σ_1	Σ_4	$-\Sigma_2$
T_{B_1}	Σ_6	0	Σ_{11}	$-\Sigma_7$	0	$-\Sigma_{10}$	$-\Sigma_4$	Σ_9	Σ_1	$B+\Delta_{B6}$	0	$-\Sigma_3$
T_{B_2}	Σ_7	0	Σ_{10}	Σ_6	0	Σ_{11}	Σ_1	$-\Sigma_3$	Σ_4	0	$B+\Delta_{B6}$	$-\Sigma_9$
T_C	Σ_8	Σ_{11}	0	$-\Sigma_5$	Σ_{10}	0	0	0	$-\Sigma_2$	$-\Sigma_3$	$-\Sigma_9$	$C+\Delta_{C2}$

substitutions

$\Delta_{A5}=(\delta^2-\gamma^2)f+\Sigma_A$
$\Delta_{B5}=-f+\Sigma_B$
$\Delta_{C5}=(\gamma^2-\delta^2)f+\Sigma_C$
$\Delta_{A1}=(\gamma^2-3\delta^2)f+\Sigma_A$
$\Delta_{C1}=(\delta^2-3\gamma^2)f+\Sigma_C$
$\Delta_{A2}=f+\Sigma_A$
$\Delta_{B6}=f+\Sigma_B$
$\Delta_{C2}=f+\Sigma_C$
$\Delta_{1+}=-\gamma 2\, f+\Sigma_1$
$\Delta_{1-}=-\gamma 2\, f-\Sigma_1$
$\Delta_2=-\gamma\delta 2\, f+\Sigma_2$
$\Delta_{3+}=-\delta 2\, f+\Sigma_3$
$\Delta_{3-}=-\delta 2\, f-\Sigma_3$
$\Delta_4=-\gamma\delta 4 f-\Sigma_2$

$\Sigma_A=P_1+P_2+\gamma^2(P_3+P_4-P_7-P_8)-2\delta\gamma(P_9+P_{10})$
$\Sigma_B=P_1+P_2+P_3+P_4+P_7+P_8$
$\Sigma_C=P_1+P_2+\delta^2(P_3+P_4-P_7-P_8)+2\delta\gamma(P_9+P_{10})$
$\Sigma_1=-\gamma P_5+\delta P_{13}$
$\Sigma_2=\gamma\delta(P_3+P_4-P_7-P_8)+(\gamma^2-\delta^2)(P_9+P_{10})$
$\Sigma_3=-\delta P_5-\gamma P_{13}$
$\Sigma_4=\gamma P'_5-\delta P'_{13}$
$\Sigma_5=-P'_6+P'_{11}$
$\Sigma_6=\delta(P_6+P_{11})-\gamma P_{12}$
$\Sigma_7=\delta(P'_6+P'_{11})-\gamma P'_{12}$
$\Sigma_8=P_6-P_{11}$
$\Sigma_9=\delta P'_5+\gamma P'_{13}$
$\Sigma_{10}=-\gamma(P'_6+P'_{11})-\delta P'_{12}$
$\Sigma_{11}=-\gamma(P_6+P_{11})-\delta P_{12}$

$B=-(a+b+c)$
$A=-(2a+b-c+\sqrt{(b-c)^2+4d^2})/2$
$C=-(2a+b-c-\sqrt{(b-c)^2+4d^2})/2$
$\gamma=2d/\sqrt{4d^2+(b-c-\sqrt{(b-c)^2+4d^2})^2}$
$\delta=-\sqrt{1-\gamma^2}$

$P_1=D_1\epsilon_{zz}$
$P_2=D_2(\epsilon_{xx}+\epsilon_{yy})$
$P_3=D_3\epsilon_{zz}$
$P_4=D_4(\epsilon_{xx}+\epsilon_{yy})$
$P_5=-D_5(\epsilon_{xx}-\epsilon_{yy})$
$P'_5=-D_5 2\epsilon_{xy}$
$P_6=D_6\sqrt{2}\epsilon_{yz}/4$
$P'_6=D_6\sqrt{2}\epsilon_{xz}/4$
$P_7=D_7\epsilon_{zz}/2$
$P_8=D_8(\epsilon_{xx}+\epsilon_{yy})/2$
$P_9=D_9\sqrt{2}\epsilon_{zz}/2$
$P_{10}=D_{10}\sqrt{2}(\epsilon_{xx}+\epsilon_{yy})/2$
$P_{11}=D_{11}\sqrt{2}\epsilon_{yz}/4$
$P'_{11}=D_{11}\sqrt{2}\epsilon_{xz}/4$
$P_{12}=D_{12}\epsilon_{yz}/2$
$P'_{12}=D_{12}\epsilon_{xz}/2$
$P_{13}=-D_{13}\sqrt{2}(\epsilon_{xx}-\epsilon_{yy})/2$
$P'_{13}=-D_{13}\sqrt{2}\epsilon_{xy}$

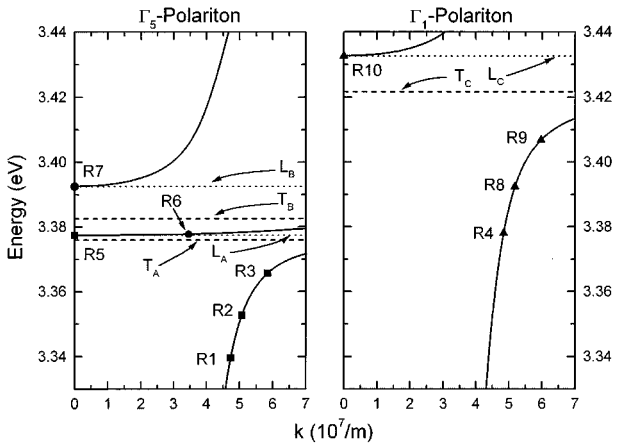

FIG. 2. Polariton dispersion curves of ZnO at zero stress (taken from Ref. 17). Squares, circles, and triangles refer to resonances of the $A(\Gamma_5)$, $B(\Gamma_5)$, and $C(\Gamma_1)$ states, respectively, measured by three-photon difference frequency generation and two-photon excitation spectroscopy. Γ_5 and Γ_1 denote the symmetry of eigenstates with polarization parallel (Γ_5) and perpendicular (Γ_1) to the z axis. T: transversal exciton, L: longitudinal exciton.

Γ_2 and Γ_6 states are pure triplet states (paraexcitons) and spin forbidden. Paraexcitons have no oscillator strength for electric dipole transitions. Γ_1 and Γ_5 states are singlet-triplet mixed states (orthoexcitons) and refer to eigenstates with polarization *parallel* (Γ_1) and *perpendicular* (Γ_5) to the z axis. Orthoexcitons are dipole allowed and thus interact with photons and form polaritons. Since in ZnO the spin-orbit coupling is small compared to the crystal-field splitting the $A(\Gamma_1)$ and $C(\Gamma_5)$ states are weakly allowed states whereas $A(\Gamma_5)$, $B(\Gamma_5)$, and $C(\Gamma_1)$ are strongly allowed orthoexcitons.[13]

For the theoretical analysis of the data we treat the stress dependence of the twelve $1S$ excitons by perturbation theory. The unperturbated Hamiltonian H^0 consists of five terms:

$$H^0 = -a\,\tfrac{1}{2}\ell_h^2 - b\ell_{h,z}^2 - c2\sigma_{h,z}\ell_{h,z} - d\sqrt{2}(\sigma_{h,x}\ell_{h,x} + \sigma_{h,y}\ell_{h,y}) + f4\vec{\sigma}_e\vec{\sigma}_h. \quad (4)$$

ℓ_h, σ_h, and σ_e are the angular momentum and the spin operators for the hole and the electron, respectively. The Hamiltonian includes parameters for the absolute energy reference (a), the crystal-field splitting (b), the anisotropic spin-orbit parameters (c and d) and isotropic analytical exchange (f).

$H^{\tau 1}$ and $H^{\tau 2}$ are operators that can be derived from an invariant expansion according to Cho.[14] They take into account the stress dependence of crystal-field splitting and spin-orbit coupling, respectively:

$$H^{\tau 1} = D_1\epsilon_{zz} + D_2(\epsilon_{xx}+\epsilon_{yy}) + [D_3\epsilon_{zz} + D_4(\epsilon_{xx}+\epsilon_{yy})]\ell_{h,z}^2 + D_5((\epsilon_{xx}-\epsilon_{yy})(\ell_{h,y}^2 - \ell_{h,x}^2) - 4\epsilon_{xy}[\ell_{h,y},\ell_{h,z}]) + D_6(\epsilon_{xz}[\ell_{h,x},\ell_{h,z}] + \epsilon_{yz}[\ell_{h,y},\ell_{h,z}]), \quad (5)$$

$$H^{\tau 2} = [D_7\epsilon_{zz} + D_8(\epsilon_{xx}+\epsilon_{yy})]\sigma_{h,z}\ell_{h,z} + [D_9\epsilon_{zz} + D_{10}(\epsilon_{xx}+\epsilon_{yy})](\sigma_{h,x}\ell_{h,x} + \sigma_{h,y}\ell_{h,y}) + D_{11}(\epsilon_{xz}\sigma_{h,z}\ell_{h,x} + \epsilon_{yz}\sigma_{h,z}\ell_{h,y}) + D_{12}(\epsilon_{xz}\sigma_{h,x}\ell_{h,z} + \epsilon_{yz}\sigma_{h,y}\ell_{h,z}) + D_{13}[(\epsilon_{xx}-\epsilon_{yy})(\sigma_{h,y}\ell_{h,y} - \sigma_{h,x}\ell_{h,x}) - 2\epsilon_{xy}(\sigma_{h,y}\ell_{h,x} + \sigma_{h,x}\ell_{h,y})], \quad (6)$$

where

$$[\ell_{h,i},\ell_{h,j}] = \tfrac{1}{2}(\ell_{h,i}\ell_{h,j} + \ell_{h,j}\ell_{h,i}). \quad (7)$$

TABLE III. Parameters of ZnO used in the theory for comparison with the experimental data.

Γ_5-polariton parameters[a]			Γ_1-polariton parameters[a]			Elastic constants[b]		
$T_{A(\Gamma_5)}$	(eV)	3.375 99±0.000 03	$T_{C(\Gamma_1)}$	(eV)	3.421 62±0.000 01	S_{11}	(10^{-11} Pa−1)	0.7858
$F_{A(\Gamma_5)}$	(eV^2)	0.161±0.005	$F_{C(\Gamma_1)}$	(eV^2)	0.540±0.006	S_{12}	(10^{-11} Pa^{-1})	−0.3432
$T_{B(\Gamma_5)}$	(eV)	3.382 56±0.000 06	$T_{b(\Gamma_1)}$	(eV)	3.561±0.001	S_{13}	(10^{-11} Pa^{-1})	−0.2206
$F_{B(\Gamma_5)}$	(eV^2)	0.360±0.005	$F_{b(\Gamma_1)}$	(eV^2)	3.05±0.06	S_{33}	(10^{-11} Pa^{-1})	0.6940
$T_{b(\Gamma_5)}$	(eV)	3.527±0.001	$\varepsilon_{b(\Gamma_1)}$		3.754±0.003	S_{44}	(10^{-11} Pa^{-1})	2.357
$F_{b(\Gamma_5)}$	(eV^2)	2.90±0.05						
$\varepsilon_{b(\Gamma_5)}$		3.658±0.003						

Exciton energies[a]			Hamilton parameters[a]			Ratio of the dipole matrix elements[a]	
A	(eV)	3.3757±0.0002	a	(eV)	−3.4180±0.0006	$\lvert M_\perp/M_\parallel\rvert$	0.98(1)
B	(eV)	3.3817±0.0002	b	(meV)	38.3±0.9		
C	(eV)	3.4199±0.0002	c	(meV)	−2.1±0.3		
			d	(meV)	−9.1±0.9		
			f	(meV)	−0.61±0.02		
			γ		−0.978±0.007		
			δ		−0.21±0.03		

[a]References 13 and 17; two- and three-photon spectroscopy at $T=5$ K.
[b]Values taken from Ref. 19.

TABLE IV. Polariton resonances $R1,...,R10$ measured by two-photon excitation spectroscopy (2P-ES) and three-photon difference frequency generation (3P-DFG). $\hbar\omega_i$ and λ_i denote the energy and wavelength of the fixed frequency laser for 3P-DFG measurements.

		3P-DFG		
Exciton	2P-ES	$\hbar\omega_1=1.16475$ eV $\lambda_1=1064.18$ nm	$\hbar\omega_2=0.80343$ eV $\lambda_2=1542.77$ nm	$\hbar\omega_3=0.649\,72$ eV $\lambda_3=1907.75$ nm
$A(\Gamma_5)$	$R5$	$R3$	$R2$	$R1$
$B(\Gamma_5)$	$R6$, $R7$			
$C(\Gamma_1)$	$R10$	$R9$	$R8$	$R4$

$D_1,\ldots,D_{13}$ denote the deformation potentials. ϵ_{ij} are the components of the strain tensor, which depend on the magnitude of the uniaxial stress τ, the stress direction and the elastic constants S_{11}, S_{12}, S_{13}, S_{33}, and S_{44} (Table I).

We calculate the matrix elements of the total Hamiltonian

$$H=H^0+H^{\tau 1}+H^{\tau 2}. \tag{8}$$

For the resulting 12×12 matrix we choose as a basis a set of wave functions that are classified by the symmetry and the Cartesian characters of the ($\ell=1$) functions. The wave functions are given in detail in Ref. 13. Table II presents the resulting Hamilton matrix. The Hamiltonian that includes nondiagonal exchange and strain terms is diagonalized. The twelve exciton eigenfunction $|\Psi_m\rangle$ corresponding to the eigenvalues E_m are linear combinations of the base functions:

$$\begin{aligned}|\Psi_m\rangle=&\lambda_{m1}|X_A\rangle+\lambda_{m2}|X_B\rangle+\lambda_{m3}|X_C\rangle+\lambda_{m4}|Y_A\rangle+\lambda_{m5}|Y_B\rangle\\&+\lambda_{m6}|Y_C\rangle+\lambda_{m7}|Z_A\rangle+\lambda_{m8}|Z_C\rangle+\lambda_{m9}|T_A\rangle\\&+\lambda_{m10}|T_{B_1}|\rangle+\lambda_{m11}|T_{B_2}\rangle+\lambda_{m12}|T_C\rangle,\end{aligned} \tag{9}$$

$$m=1,\ldots,12.$$

X, Y, Z denote the polarization of the singlet part of the base wave functions and T denotes pure triplet states. From the eigenfunctions Ψ_m one can calculate relative matrix elements $\langle 0|\hat{D}|\Psi_i\rangle$ for the allowed transitions, where $\hat{D}$ is the dipole operator and $|0\rangle$ corresponds to the ground state:

$$\begin{aligned}|\langle 0|\hat{D}|\Psi_m\rangle|^2=1/2[&(\lambda_{m1}\gamma+\lambda_{m2}+\lambda_{m3}\delta)^2+(\lambda_{m4}\gamma+\lambda_{m5}\\&+\lambda_{m6}\delta)^2]M_\perp^2+(\lambda_{m7}\delta+\lambda_{m8}\gamma)^2M_\parallel^2,\end{aligned} \tag{10}$$

where

$$M_\perp=\langle 0|\hat{D}|xs\rangle=\langle 0|\hat{D}|ys\rangle,\quad M_\parallel=\langle 0|\hat{D}|zs\rangle. \tag{11}$$

s is the singlet state $[(\uparrow_e\downarrow_h-\downarrow_e\uparrow_h)/\sqrt{2}]$ and x, y, z denote the directions of the ℓ functions. The parameters γ and δ depend on the crystal-field and spin-orbit parameters and are defined in Table II.

The eigenvalues E_m of the Hamiltonian Eq. (8) and the matrix elements Eq. (10) determine the exciton oscillator strengths F_m for a given value and direction of the stress:[15]

$$F_m\propto E_m|\langle 0|\hat{D}|\Psi_m\rangle|^2,\quad m=1,\ldots,12. \tag{12}$$

This procedure leads to the components $\varepsilon_{ii}(i\in\{1,2,3\})$ of the dielectric tensor, which has only diagonal components in the system of principal axes:

$$\varepsilon_{ii}(E)=\varepsilon_{b,i}+\sum_n \frac{F_{i,n}}{E_{i,n}^2-E^2}, \tag{13}$$

$\varepsilon_{b,i}$ are the background dielectric constants. The sum in Eq. (13) is extended over all eigenstates with a polarization parallel to the corresponding principle axis.

The resonances on the polariton dispersion curves can be calculated by solving the macroscopic Maxwell equations as described in Ref. 16. For stress direction [0001] the dielectric tensor consists of two different diagonal elements and the

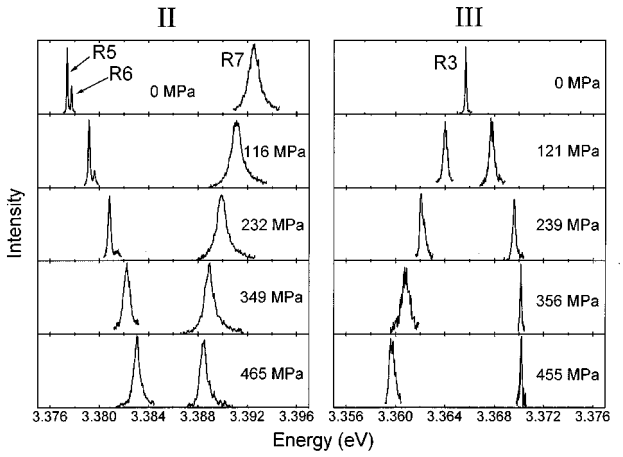

FIG. 3. Stress-induced shift and splitting of resonances R_3, R_5, R_6, and R_7 (cf. Fig. 1). Resonance R_3 is measured by three-photon difference frequency generation whereas resonances R_5, R_6, and R_7 are derived by two-photon excitation spectroscopy.

TABLE V. Deformation potentials of ZnO. The different conventions for the definition of the deformation potentials in the stress Hamiltonian are taken into account.

Deformation potential	This work	Euwema *et al.*[a]
D_1 (eV)	-3.90 ± 0.03	-3.8
D_2 (eV)	-4.13 ± 0.03	-3.8
D_3 (eV)	-1.15 ± 0.04	-0.8
D_4 (eV)	1.22 ± 0.04	1.4
D_5 (eV)	1.53 ± 0.01	1.2
D_6 (eV)	2.88 ± 0.04	2.8

[a]Reference 9; reflection under uniaxial stress at $T=1.8$ K.

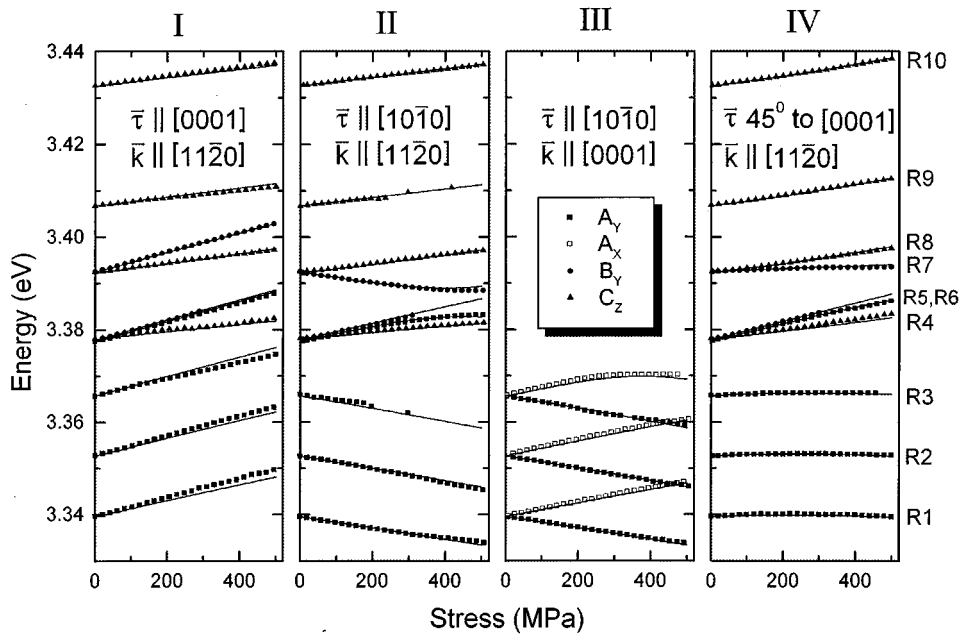

FIG. 4. Stress-dependent shift and splitting of resonances $R_1,\ldots,R_{10}$ for configurations I–IV. The solid lines are the result of a least-squares fit and symbols denote experimental results.

crystal is uniaxial, whereas for other stress directions all components are different and the crystal becomes biaxial:

$$\hat{\varepsilon}=\begin{pmatrix} \varepsilon_{11} & 0 & 0 \\ 0 & \varepsilon_{22} & 0 \\ 0 & 0 & \varepsilon_{33} \end{pmatrix}. \tag{14}$$

$\varepsilon_{11}=\varepsilon_{22}\neq\varepsilon_{33}$ for stress direction [0001], and $\varepsilon_{11}\neq\varepsilon_{22}\neq\varepsilon_{33}\neq\varepsilon_{11}$ for other stress directions. In all stress configurations (cf. Fig. 1) the total $\vec{k}$ vector is parallel to a principal axis of the dielectric tensor and Maxwell's equations lead to the dispersion formula of pure transverse and longitudinal waves:

$$\varepsilon_{ii}=\frac{k^2c^2}{\omega^2} \quad \text{for transverse states,} \tag{15}$$

$$\varepsilon_{ii}=0 \quad \text{for longitudinal states.} \tag{16}$$

IV. RESULTS AND DISCUSSION

Figure 2 shows the polariton dispersion curves of ZnO without external perturbation and the measured polariton resonances (taken from Ref. 17). The two polariton dispersions are classified by eigenstates with a polarization perpendicular (symmetry Γ_5) and parallel (symmetry Γ_1) to the z axis, respectively. We have used Sellmeyer formulas with three and two oscillators [orthoexcitons and phenomenological background oscillators $b(\Gamma_5)$ and $b(\Gamma_1)$ which represent resonances at higher energies]:

$$\frac{\hbar^2c^2k^2}{E^2}=\varepsilon_{\Gamma_5}=\varepsilon_{b(\Gamma_5)}+\frac{F_{A(\Gamma_5)}}{T_{A(\Gamma_5)}^2-E^2}+\frac{F_{B(\Gamma_5)}}{T_{B(\Gamma_5)}^2-E^2}+\frac{F_{b(\Gamma_5)}}{T_{b(\Gamma_5)}^2-E^2}, \tag{17}$$

for the Γ_5 polariton and

$$\frac{\hbar^2c^2k^2}{E^2}=\varepsilon_{\Gamma_1}=\varepsilon_{b(\Gamma_1)}+\frac{F_{C(\Gamma_1)}}{T_{C(\Gamma_1)}^2-E^2}+\frac{F_{b(\Gamma_1)}}{T_{b(\Gamma_1)}^2-E^2} \tag{18}$$

for the Γ_1 polariton. We neglect damping, spatial dispersion, and the oscillator strengths of the weak allowed orthoexcitons $A(\Gamma_1)$ and $C(\Gamma_5)$ [cf. Eqs. (1) and (3)]. The parameters of the polariton dipersion are listed in Table III. The nonlinear resonances $R_1,\ldots,R_{10}$ measured by 2P-ES and 3P-DFG are well reproduced by the polariton dispersion curves cal-

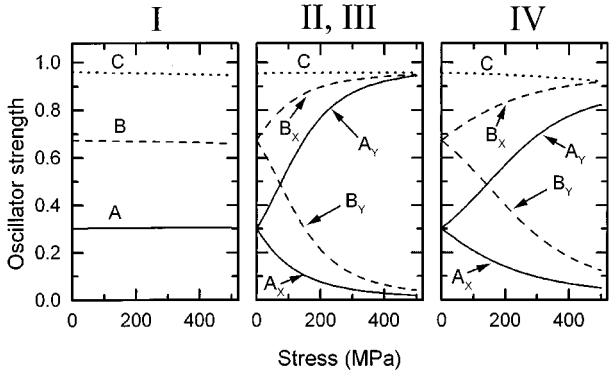

FIG. 5. Oscillator strengths for the strong allowed orthoexcitons for the stress configurations I–IV.

culated from Eqs. (17) and (18). Table IV gives an overview of the polariton resonances $R_1,\ldots,R_{10}$ and the corresponding nonlinear technique. We measured four resonances by 2P-ES and six resonances by 3P-DFG.

As an example we show in Fig. 3 the stress-induced shifts and splittings for the resonances R_3, R_5, R_6, and R_7 of configurations II and III. For this configuration the crystal becomes biaxial and thus the eigenstates, which are classified by X and Y polarization are no longer degenerate. The splitting is a combined effect of analytical exchange and stress and was discussed by Euwema *et al.*[9]

For the analysis of the experimental results under uniaxial stress we use the elastic constants, polariton and exciton parameters listed in Table III. The parameters of the Hamiltonian H^0 [Eq. (4)] of the unperturbated crystal are determined by the exciton energies and their oscillator strengths as described in Ref. 13.

According to Eqs. (5) and (6) and Table I the stress Hamiltonian depends for the configurations I, (II, III) and IV on 8 ($D_1,\ldots,D_4$, $D_7,\ldots,D_{10}$), 10 ($D_1,\ldots,D_5$, $D_7,\ldots,D_{10}$ and D_{13}), and all 13 deformation potentials, respectively. For each stress direction at least 8 deformation potentials occur in the stress Hamiltonian [Eqs. (5) and (6)]. Therefore we determined the deformation potentials by fitting the four configurations *simultaneously*. We made two different fits for the analysis of the experimental data:

In a first calculation we take into account the stress Hamiltonian according to Bir and Pikus,[18] which is identical to Eq. (5), but in this theory the stress dependence of spin-orbit parameters is neglected. Values for $D_1,\ldots,D_6$ from a least-squares fit are listed in Table V. Solid curves in Fig. 4 show the result of this fit. Good agreement with our experimental data is achieved. There is a discrepancy concerning the stress-induced shifts of the resonsances R_1, R_2, and R_3 in configuration I. One has to keep in mind that we neglect the stress dependence of the background ocillators $b(\Gamma_5)$, $b(\Gamma_1)$ and the background dielectric constants $\varepsilon_{b(\Gamma_5)}$, $\varepsilon_{b(\Gamma_1)}$ [cf. Eqs. (17) and (18)]. As shown in Ref. 11 resonances of the lower polariton branch are sensitive to the stress dependence of higher oscillators.

In a second analysis we use the total stress Hamiltonian [Eqs. (5) and (6)] for the analysis of the experimental data. This fit takes into account the stress dependence of the crystal-field splitting *and* the spin-orbit coupling. There was no significant difference as compared to the result of the first fit (Fig. 4). The total error decreases only by 9% compared to the first fit. This result gives clear evidence that the stress dependence of spin-orbit parameters can be neglected in ZnO.

Figure 5 shows the normalized oscillator strengths of the strongly allowed $A(\Gamma_5)$, $B(\Gamma_5)$, and $C(\Gamma_1)$ $1S$ excitons. For configuration I the oscillator strengths are nearly independent of the stress whereas for the other configurations a splitting of the A and B exciton oscillator strength is resolved. Due to the stress-induced mixing of A and B states the A_Y and B_X states attain oscillator strength from the B_Y and A_X states, respectively.

In Table V we compare the deformation potentials of this work with the results of Euwema *et al.*[9] who used linear reflection. There is good agreement concerning the values of D_1, D_2, and D_6. We were able to resolve a slight difference between D_1 and D_2 wheras Euwema *et al.* detemined identical values. There are significant discrepancies concerning the values of D_3, D_4, and D_5. Since the analysis of reflection spectra requires the use of Kramers-Kronig relations and since the linewidths of resonances in reflection are about ten times larger than those of the resonances of the nonlinear measurements in this work, we are convinced that our deformation potentials are more reliable.

In conclusion we have shown that nonlinear spectroscopy is a suitable technique for the determination of polariton parameters with high accuracy. Starting from the full Hamiltonian for wurtzite structure we analyzed polariton states in ZnO under uniaxial pressure up to 500 MPa. The analysis of the data shows clearly that the stress dependence of the spin-orbit splitting can be neglected in ZnO and that six deformation potentials are sufficient for the description of the experimental results.

ACKNOWLEDGMENTS

The authors thank K. Reimann and U. Rössler for stimulating discussions. The financial support of one of the authors (J.W.) by the Graduiertenkolleg ''Festkörperspektroskopie'' is greatly appreciated.

[1] S. Nakamura, M. Senoh, S. Nagahama, N. Iwasa, T. Yamada, T. Matsushita, Y. Sugimoto, and H. Kiyoto, Appl. Phys. Lett. **69**, 4056 (1996).

[2] M. A. Haase, J. Qiu, J. M. DePuydt, and H. Cheng, Appl. Phys. Lett. **59**, 1272 (1991).

[3] S. A. Ding, G. Neuhold, J. H. Weaver, P. Häberle, K. Horn, O. Brandt, H. Yang, and K. Ploog, J. Vac. Sci. Technol. A **14**, 819 (1996).

[4] K. Reimann and St. Rübenacke, Phys. Rev. B **49**, 11 021 (1994).

[5] A. Mang, K. Reimann, and St. Rübenacke, in *Proceedings of the 22nd International Conference on the Physics of Semiconductors, Vancouver*, edited by D. J. Lockwood (World Scientific, Singapore, 1995), Vol. 1, p. 317.

[6] A. Mang, K. Reimann, and St. Rübenacke, Solid State Commun. **94**, 251 (1995).

[7] D. Fröhlich and W. Nieswand, Philos. Mag. B **70**, 321 (1994).

[8] D. Fröhlich, W. Nieswand, U. W. Pohl, and J. Wrzesinski, Phys. Rev. B **52**, 14 652 (1995).

[9] R. N. Euwema, D. W. Langer, K. Era, and T. Koda, Phys. Rev. B **2**, 4005 (1970).

[10] D. C. Reynolds, D. C. Look, B. Jogai, and H. Morkoç, Solid State Commun. **101**, 643 (1997).

[11] D. Fröhlich, W. Nieswand, and St. Rübenacke, Phys. Rev. B **47**, 6736 (1993).

[12] G. F. Koster, J. O. Dimmock, R. G. Wheeler, and H. Statz, *Properties of the Thirty-Two Point Groups* (MIT Press, Cambridge, MA, 1963).

[13] J. Wrzesinski and D. Fröhlich, Solid State Commun. (to be published).

[14] K. Cho, Phys. Rev. B **14**, 4463 (1976).

[15] V. M. Agranovich and V. L. Ginzburg, *Spatial Dispersion in Crystal Optics and the Theory of Excitons* (J. Wiley & Sons, London, 1966).
[16] M. Fiebig, D. Fröhlich, and Ch. Pahlke-Lerch, Phys. Status Solidi B **177**, 187 (1993).
[17] J. Wrzesinski and D. Fröhlich (unpublished).
[18] G. L. Bir and G. E. Pikus, *Symmetry and Strain-Induced Effects in Semiconductors* (Wiley, New York, 1974).
[19] T. B. Bateman, J. Appl. Phys. **33**, 3309 (1962).